Automated Analysis of Emissivity Spectra of Au, SiN, and SiO_2 Nanoparticles Using Machine Learning

Samuel Gleason
College of Chemistry
University of California, Berkeley
smglsn12@berkeley.edu

Chloe Hsu
Department of Electrical Engineering
Computer Science
University of California, Berkeley
chloehsu@berkeley.edu

Abstract

A crucial step in nanoparticle synthesis is to verify whether the synthesized particles are of the desired shapes and sizes, since nanoparticles' morphology largely determine their function. Currently, such verification depends on complex and time-consuming analytical measurements.

To simplify the measurement procedure, we show that machine learning models can effectively predict nanoparticles' shapes and sizes based on their emissivity spectra. The emissivity spectra reflect particles' optical properties, and are simpler to measure than direct size measurements with more advanced techniques such as transition electron microscopy (TEM). As optical properties are determined by particle shapes and sizes, machine learning models can extract morphology information from emissivity spectra.

We compare the effectiveness of three types of models: random forests, fully connected neural networks, and convolutional neural networks, and compare different training procedures. We find that a ResNet-based convolutional neural network performs the best on shape classification, while random forests and convolutional neural networks are comparable on size regression. We also include studies on the effects of data augmentation, multi-task training, and joint training on materials.

1 Introduction

Nanoscale materials find applications in diverse areas, from conversion of light into electricity in solar cells to the visualization of cancer cells. Nanoparticles are broadly defined as particles that have dimensions in the nanometer range. In most nanoparticle applications it is crucial to synthesize nanoparticles of specific sizes and shapes.

Gold nanoparticles and LSPR Gold nanoparticles (Au NPs) have applications in drug delivery and biological imaging due to their stability and low toxicity [1]. They also have significant applications in solar cells, for example as light trapping devices in organic solar cells [2].

These applications take advantage of a property of metal nanoparticles called localized surface plasmon resonance (LSPR). LSPR is observed when light strikes a metal nanoparticle, causing electron density in the particle to be polarized to one surface and oscillate in accordance with the light's wavelength. This electron oscillation is highly dependent on the size and shape of the nanoparticle, which can be intuitively thought of as dictating the distance and dimension of a full electron cloud oscillation. Some specific wavelengths, called resonant frequencies, cause standing oscillations of electron density, which greatly enhance the metal particle's absorbance of light. The length of electron oscillation, and therefore the particle's size and shape, is highly correlated with that particle's resonant frequency [3] . As many of the applications of Au NPs involve engineering

Preprint. Under review.

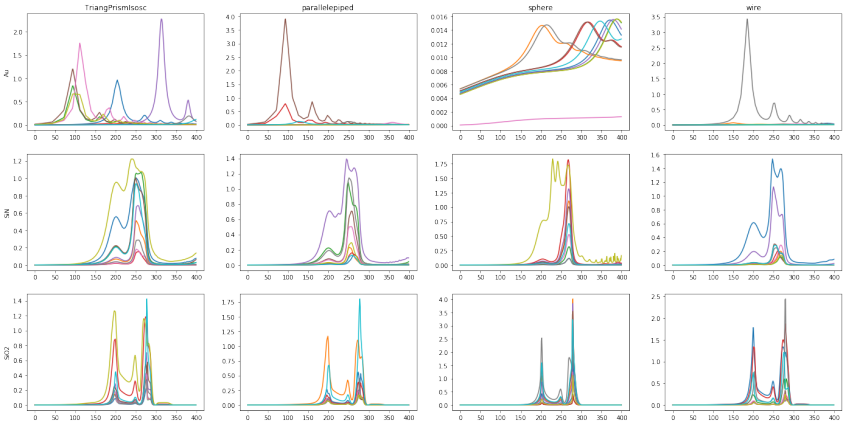

Figure 1: 10 randomly sampled emissivity spectra from each class in the training data. The columns are the four shapes: triangular prisms, parallelepipeds, sphere, and wire. The three rows are the three materials: Au, SiN, and SiO_2.

particles that either strongly absorb or emit light at specific wavelengths, such as those described above, creating Au NPs with specific sizes and shapes is of paramount importance for nanoscience researchers.

SiO_2 and SiN nanoparticles Silicone dioxide (SiO_2) and silicon nitride (SiN) nanoparticles have also been the subject of increasing research. Both of these materials have many applications to solar technology [4, 5], which, similar to Au NPs, depend heavily on their optical properties. Unlike Au NPs, SiN and SiO_2 are not metal nanoparticles and therefore do not experience LSPR. Their absorption and emission of light depends on transitions to different electronic and vibrational energy levels. Despite this, the optical properties of SiN and SiO_2 nanoparticles depend on shape and size. Elzouka et al [6] showed the size of SiO_2 and SiN nanoparticles are correlated to their emissivity, showing emissivity, itself an optical property and directly connected to absorbance, is connected to size and shape of SiN and SiO_2 particles. Therefore, as with Au NPs, creating SiN and SiO_2 NPs with specific sizes and shapes is incredibly important to nanoscience researchers.

Emissivity spectra A particle's emissivity spectrum is one of many experimental analytical methods researchers use to determine the sizes and shapes present is a nanoparticle sample. Emissivity, which is broadly defined as the emission of energy as thermal radiation by a material, is highly dependent on the chemical composition, size, and shape of nanoparticles [7]. This clear connection between a particle's emissivity and its size/shape makes emissivity a good candidate for building models to automate the analysis of sizes and shapes in nanoparticle samples. Additionally, particle emissivity can be simulated by numerically solving Maxwell's Equations [6], which allows the construction of a large volume of training data for machine learning models.

Inverse problem: estimation shape and size from emissivity spectra Determining the sizes, shapes, and materials of nanoparticles present in a sample, with the level of detail needed for the applications described above, can be complicated from simply looking at the emissivity spectrum of a sample. This is especially true for size applications, which can require size specified to the nanometer. Usually, researchers are required to turn to more complicated and time consuming methods, such as transition electron microscopy (TEM), to attain this level of detail. Here we create a model to conduct automated analysis of emissivity spectra and provide the shape and size detail that usually requires more sophisticated, and time consuming, analysis. In this report, we refer to spectral prediction as the forward problem (particle details as inputs, emissivity spectra as outputs), and refer to material and geometry inference as the inverse problem (emissivity spectra in, particle details out).

Our contribution In this study, we build an inverse model as an experimental analytics tool, where a user can input an experimental emissivity spectrum of a nanoparticle sample and determine the shape, size, and material of their sample. We directly train an inverse model with training data from numerical simulations. As data augmentation for the training data, we also use the forward model

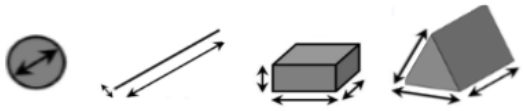

Figure 2: Four nanoparticle shapes in the dataset: spheres, wires, parallelepipeds, and triangular prisms with arrows showing the distinct dimensions of each shape. A sphere has only one distinct dimension (its diameter in this case) and therefore the shortest, middle, and longest dimensions are all the same. Wires have two dimensions, the diameter and length of the wire, and in this dataset the shortest and middle dimensions represent the diameter of the wire and the longest dimension reflects the length of the wire. Triangular prisms and parallelepipeds have three distinct dimensions.

trained in [6] to generate additional training data. The data augmentation step can likely be skipped when more numerical simulation data is available[1]. We compare random forests and 5 neural network architectures including fully connected networks and convolutional neural networks. We provide the first machine learning based inverse models for automated emissivity spectrum analysis. Our models achieve 85.9% top-1 accuracy on shape classification and 0.91 correlation on size regression.

2 Related work

Most related to our work, Elzouka et al. [6] studied a different approach to the inverse problem: train a decision tree model for the forward problem, and perform inverse design by specifying a spectrum, finding the output leaf on the decision tree whose value corresponds closest to the target spectrum, and then tracing up the decision tree to find a range of sizes, shapes, and materials that reasonably approximate that spectrum. Elzouka et al. [6] were motivated by the inverse design task in an engineering context, where the goal was to return the specifications of materials that best fit the given optical properties. However, their model is not optimized for automated spectrum analysis.

There are two key differences between the inverse design task and the automated analysis task. First, inverse design models return multiple particle specs or a range of specs that would have similar properties to a target spectrum, rather than providing detailed information about the assignment of a spectrum. Second, the accuracy measurements are different. In inverse design, the accuracy is measured in the spectrum space (by comparing target spectrum to the spectra of the predicted particles). In contrast, as an automated analytical tool, our model is optimized for accuracy in the nanoparticle parameter space to ensure the predicted particle's size, shape, and material most closely match the true particle parameters. These differences in context requires a new model for the inverse problem as an automated analysis tool.

In addition to [6], He et al. [8] use 2-layer fully connected neural networks for both forward prediction of optical properties and inverse prediction of nanoparticle dimension parameters. He et al. focus on size regression of gold particles. We study a more general prediction problem on a larger dataset (their dataset contains 3118 nanoparticles and 57 points on each spectrum), and also compare more diverse machine learning models.

3 Problem setup

Dataset Construction Our dataset was constructed by solving Maxwell's equations to predict emissivity spectra of 15626 particles of varying materials, shapes, and sizes. This numerically solved data was taken from [6] with permission from the authors. The materials present are gold (Au), silicone dioxide (SiO_2), and silicon nitride (SiN). The shapes present are triangular prisms, parallelepipeds, spheres, and wires, as shown in Figure 2. The size of each particle is represented by four parameters: the log of the area over volume, and the shortest, middle, and longest dimensions of the particle. See Figure 2 for annotations about the dimensions of each shape. Figure 6 in the appendix shows the distribution of the geometric parameters.

[1]Due to the shelter-in-place order, we were unable to obtain additional numerical simulation data, and thus chose to instead use the data generated by the forward model.

The emissivity spectrum of each nanoparticle is represented by the emissivity at 400 different angular frequencies, chosen in a logarithmic spacing from 10^{13} rad/s to 0.8×10^{14} rad/s. These angular frequencies can be converted to wavelengths, and represent a wavelength region from roughly 1900 to 19000 nm, meaning these emissivity values are located in the infrared region. Figure 1 visualizes example spectra from each shape and material.

Prediction task Given the 400-point emissivity spectrum as input, we want to predict the shape, material, and dimensions (size) of the nanoparticle. We measure classification performance by top-1 accuracy, and we measure size regression performance by mean square error (MSE).

Data augmentation The numerically simulated dataset of 15,900 points was used to train a forward design model, which took a particle's material, shape, and size as input and predicted its emissivity spectrum (this is the same forward design model used in [6] and was shown by them to be highly accurate at predicting spectra from particle properties). This model was then used to predict spectra for $20 \times 7650 \approx 160,000$ particles. This much larger RF-labeled dataset was used to augment the training data for our models. For neural network models, we also report ablation studies of varying augmented data size (up to 600$\times$ the original data size, 300×7950 = 2.4M data points) to investigate the effects of data augmentation.

Data split We use the data from the forward design model plus 50% of the numerical simulation data (7950 points) for training, 25% of the data (3975 points) for validation, and the remaining 25% (3975 points) for test. All of the validation and test data points are from the numerical simulation to ensure meaningful model evaluation.

4 Random forests

Random forest classifiers from the scikit-learn package [9] are used to predict material, shape, and mixture composition from spectra. Random forest regression models [9] are used to predict the size parameters from spectra.

Shape Classification Two types of models were created to predict shape from spectra: binary classification models, where the task was to predict whether the sample was a particular shape depending on its spectrum, and multiclass models, where the task was to assign the inputted spectrum to one of the four shapes. Four binary classification models were trained, one for each shape. The training and test sets for each binary classification model were built by taking a random subset of the full dataset, such that the random subset would be a 50/50 split between the shape of interest and the other three shapes. This was done to prevent potential bias in the model from having an unequal split between categories. Both binary and multiclass models used 50 trees and were trained on datasets boostrapped from the full dataset, with 20 of the 400 spectral inputs available for each tree. Changing other hyperparameters from sklearn defaults did not improve model performance, and therefore were left at their default values.

Material Classification To predict material from spectra, a random forest classifier with 50 trees and 20 of the 400 spectral inputs available for each tree was used. No additional exploration was done on this model since the first model produced 100 percent accuracy.

Size Regression The size regression model used a multioutput regression model to train a model capable of predicting all four size parameters simultaneously. 50 trees trained on datasets boostrapped from the full dataset were used to create this model. As with the shape classification models, 20 of the 400 spectral inputs were available for each tree with the rest of the hyperparameters left at their default values.

5 Neural networks

Fully-Connected Networks We include three types of fully-connected networks in our model comparison: a one-layer neural network with 512 hidden units, a two-layer neural network with 512 and 128 hidden units, and a three-layer neural network with 512, 256, and 64 hidden units. All of them use dropout and ReLU activation.

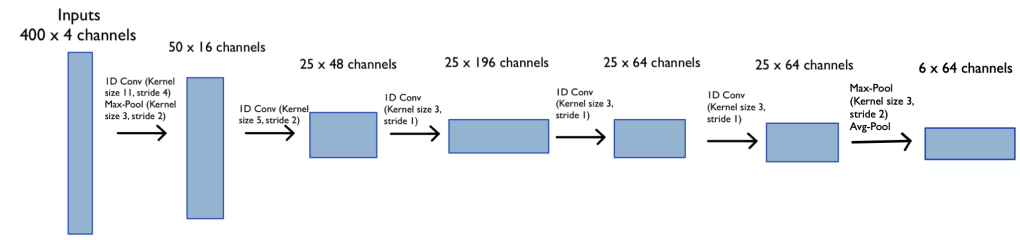

Figure 3: Adapted 1D convolutional neural network architecture from AlexNet.

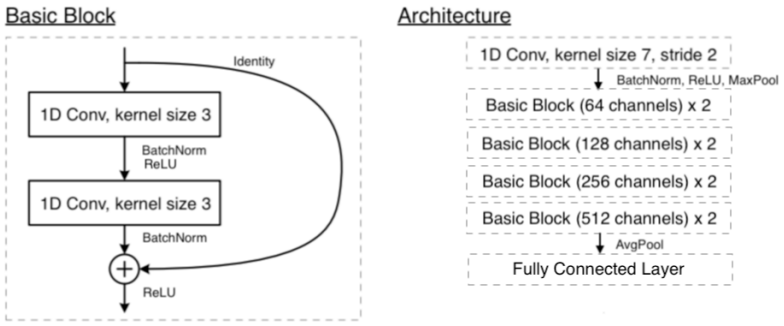

Figure 4: Adapted 1D convolutional neural network architecture from ResNet18.

Convolutional Neural Networks We adapt the popular AlexNet [10] and ResNet [11] architectures from the computer vision community by replacing 2D-convolutions with 1D-convolutions. The adapted architectures are illustrated in Figure 3 and Figure 4. For AlexNet, we keep the kernel size and stride fixed from the original AlexNet architecture, but reduce the number of channels. For ResNet, we replace the 3x3 2D-convolution with 1D-convolution of kernel size 3 in the basic block. and keep the overall ResNet-18 architecture.

Inputs and Outputs In addition to the 400-point emissivity data, we also include log emissivity, and the finite-difference derivatives of emissivity and log emissivity in the inputs. To investigate the effects of including the additional features, we report ablation result in Table 1 for ResNet18-1D on only raw emissivity data as "ResNet18-1D (1 channel input)".

For fully-connected networks, the inputs are $(\text{batch size}) \times 1600$ vectors with the 4 features flattened. For convolutional neural networks, the inputs are $(\text{batch size}) \times 4 \times 400$ vectors with 4 channels representing the emissivity, log emissivity, and their finite-difference derivatives.

For shape classification or size regression, the neural networks output 4 logits, and for joint multi-task training, the neural networks output 11 logits (4 for shape classification, 3 for material classification, and 4 for size regression).

Hyperparameters After a coarse hyperparameter search (due to limited computing resources), we use Adam optimizer with learning rate 1e-4 and batch size 64 for 20 epochs.

6 Results

6.1 Material Classification

Material classification proved very easy for random forest models as well as neural networks. The random forest model produced 100 percent classification accuracy and most neural networks attempted also achieve >99% material classification accuracy.

Model	Classification Top-1 Accuracy				
	Triangle Prism	Parallelpiped	Sphere	Wire	Average
Random guess	0.25	0.25	0.25	0.25	0.25
Random forest	0.72	0.63	0.99	0.78	0.78
One-layer neural network	0.549	0.177	0.938	0.578	0.561
Two-layer neural network	0.645	0.216	0.919	0.478	0.565
Three-layer neural network	0.615	0.177	0.938	0.486	0.554
AlexNet-1D	0.487	0.385	0.997	0.796	0.667
ResNet18-1D	0.803	0.768	0.997	0.867	**0.859**
ResNet18-1D (1-channel input)	0.762	0.691	0.993	0.888	0.834

Table 1: Shape classification top-1 accuracies when trained on all materials combined.

6.2 Shape Classification

In the shape classification task, the models predict which of the four shapes a spectrum corresponds to. Model performance, as measured by top-1 accuracy, is shown in Table 1. Additionally, we include the confusion matrix between shapes in Figure 7 in the appendix, and also report top-1 accuracy of shape classification results when trained and tested only on Au nanoparticles in Table 5 in the appendix.

In addition to 4-way shape classification, the random forest binary classification models show accuracies of 0.817, 0.739, 0.998, and 0.812 for triangle prism, parallelpiped, sphere, and wire respectively, as illustrated in Figure 8 in the appendix. Compared to 4-way classification, binary classification is easier for random forest models to learn.

6.3 Size Regression

Random forests and ResNet18-1D are comparable in size regression when measured by mean square error, as shown in Table 2. The overall 3.99 MSE of the random forest model corresponds to a 0.91 correlation between the predicted values and the true values, making the model a useful tool for examining particle dimensions.

When random forest regression is broken down by shape the triangular prism had by far the largest MSE (6.08), nearly twice the size of wire (3.66) and over twice parallelepiped (2.85). As with shape classification, the sphere size regression was essentially perfect, with a MSE of 0.004. Plots showing the correlation and MSE of the four separate shapes for the size regression task are shown in Figure 9 in the appendix. We also show the histogram of random forest regression residuals squared in Figure 10 in the appendix. This plot shows that the random forest largest dimension size regression model's large MSE is driven by a small percentage of the predicted points that have very high residuals. Although the MSE for this model is 16.1, the median squared residual is only 5.3, showing the impact of a few large errors on the MSE of this model.

Model	Mean Square Error			
	Short Dim	Middle Dim	Long Dim	log Area/Vol
Random forest	**0.068**	0.296	16.113	**0.029**
One-layer neural network	0.269	1.517	31.334	0.182
Two-layer neural network	0.252	1.894	32.443	0.302
Three-layer neural network	0.289	2.177	31.987	0.372
1DAlexNet	0.317	1.408	18.003	0.307
1DResNet-18	0.098	**0.263**	**11.414**	0.055

Table 2: Size regression mean square error.

6.4 Additional Studies on Training Procedure

Multi-task training We experiment with multi-task training by using a multi-head model to predict shape classification, material classification, and size regression at the same time. Our results in Table 3 show that the additional tasks do not increase or decrease shape classification performance.

	Shape Classification Top-1 Accuracy		Size Regression Average MSE	
	Single-Task	Multi-Task	Single-Task	Multi-Task
ResNet18-1D	**0.859**	0.818	**2.958**	3.466

Table 3: Comparison of multi-task vs single-task training.

Joint training on materials When we compare joint training on all three materials together against training separate models for each material, we find no significant difference in model performance, as shown in Table 4.

	Separate Training				Joint Training
	Au	SiN	SiO_2	Avg	
ResNet18-1D Top-1 Shape Accuracy	0.770	0.869	0.927	0.855	0.859

Table 4: Comparison of joint training on all materials versus separate training for each material.

Effects of data augmentation As shown in the scatter plot in Figure 6 in the appendix, 10x data augmentation is crucial for achieving the best shape classification performance on ResNet18-1D, but beyond that model performance does not increase with more data augmentation.

7 Discussion

Material classification Our material classification models attain >99% accuracy across model types. From Figure 1, it is clear that the SiO_2 and SiN particles all have roughly similar features in their spectra, making them easy to separate from each other. The Au particle spectra features are less consistent across shapes, but significantly different from the SiN and SiO_2 particle spectra. This has important implications for our shape classification models. Since the materials are clearly distinct, the shape classifiers effectively only have to classify shape within one material. For example, an SiO_2 sphere is realistically only likely to be confused with other SiO_2 shapes. This also explains the result in Table 4 that joint training on all materials gives roughly the same result as training separately.

Shape classification ResNet18-1D, an adapted 1D convolutional neural network architecture from ResNet18, is most effective for shape classification. ResNet is known to have good image classification performance due to convolutions and the residual connections, which likely also contributed to its effectiveness on shape classification. A possible explanation for why the random forest models struggled with shape classification comes from examining the feature importance, as shown in Figure 12. Random forest models excel when different classes have distinctive features that can be used to separate them from each other. However, when examining the feature importance for shape classification, it can be seen that none of the wavelengths stand above the others in terms of effectiveness. Therefore, it is unsurprising that random forest models are outperformed by more sophisticated neural networks, which are able to extract more detailed information.

Sphere classification was nearly perfect, and the confusion matrix from the random forest multiclass model shows the other three shapes were rarely misclassified as spheres. Therefore, the emissivities of spheres contain distinct features from the other three shapes. This observation makes sense for Au spheres, since their spectra are radically different from the other Au particles in Figure 1. However, at first glance it is not as clear that why spheres are so easy to classify for SiN and SiO_2, since the spectra of spheres are not as distinct. To explain this observation, a feature importance graph for the random forest sphere binary classifier was made Figure 13. This plot shows that the wavelength at index 269 is the most important parameter, as well as the wavelengths between 260 and 280. For SiO_2 spheres it is clear that the increased intensity in this region relative to the other SiO_2 shapes explains this region's usefulness (Figure 1). For SiN, the sphere spectra between 260 and 280 are much sharper than the other SiN shapes, further explaining how these parameters differentiate spheres from the other three shapes. The wavelength at 307 is likely used to separate gold spheres from most of the other shapes/material combinations, since it is rare for any of the other combinations to have intensity in this region (Figure 13). These findings suggest that experimentalists attempting to

synthesize nanospheres will be able to easily differentiate their intended product from other shapes produced using emissivity spectra, if those shapes are wires, parallelepipeds, or triangular prisms.

Similarly, Figure 1 helps explain why wires and parallelepipeds are commonly misclassified as each other. Across all three materials, even a random sample has selected spectra that contain very similar features. This is supported by examining the feature importance plot for the wire and parallelepiped binary classification models. These two plots (figure 14) show that many of the same features are important to both models, mainly regions 190-210 and 260-280. From examining figure 1, it is clear that the spectra for wires and parallelepipes are similar in this region, and therefore using these wavelengths to separate the two shapes is likely challenging. The model is likely using these wavelengths to separate these two shapes from the other shapes and then struggling to decide if the spectrum pertains to a wire or parallelepiped. This difficulty in separating wires and parallelepipes suggests that experimentalists should try to avoid using syntheses that could produce either of these shapes, since determining which they have is likely to be a challenge.

Size regression Random forest regression models out-performed neural networks in two of the four size parameters, short dimension and log(area/volume), and were essentially tied with the best neural network at predicting the middle dimension. The only size parameter where random forests were clearly outperformed was the longest dimension. An explanation for the success of these random forest models can be found in the feature importance plots of the models used to predict these four parameters (fig 11). For log(area/volume) and shortest dimension, random forests are clearly successful due to the ability of a couple wavelengths to determine size. Both models found that a particular wavelength was extremely good at separating the dataset, and is therefore has a feature importance of over 0.4. This is in contrast with the shape classification model, where no wavelength had an importance greater than 0.04. Not only does this result explain the success of random forest models, but it also represents an interesting fundamental nanoscience discovery. The knowledge that the wavelengths at indices 293 and 269 contain a huge amount of information for determining log(area/volume) and the shortest dimension of the nanoparticle, respectively, can help experimental nanoscientists build increased understanding of how emissivity at certain wavelengths is connected to the sizes of nanoparticles. Similarly, it is a striking observation that the peak wavelength on the shortest dimension model is the same as the peak in the sphere classification model, wavelength 269. This observation provides information about what emissivity wavelengths are distinct to spheres and also suggests correlations between predicting shortest dimension and sphere classification. Based on their accuracy and interpretability relative to neural networks, random forest models appear to be the best choice for size classification of nanoparticles from emissivity spectra.

When investigating training procedures, we find that multi-task training (material and shape classification + size regression) leads to worse performance than single-task training, and find no significant difference between training for all materials together and training for the three materials separately. Data augmentation by a forward model helps boost inverse model performance, with up to 10x data augmentation ratio, while further data augmentation does not lead to further performance increase. Given the high amount of variability observed in the spectra, even within the same material and shape combination, it is unsurprising that increased data improves performance. It is also possible that past 10x data augmentation we are running into the limits of our forward design model to produce distinct spectra for particles with the same material, geometry, and very slightly different sizes, which might explain why increasing data past this point doesn't further improve model performance.

8 Conclusion

Machine learning for material simulation and analysis is an exciting research direction. We have built models capable of reliably predicting material, size, and shape of nanoparticles from their emissivity spectra. After testing many model types on these prediction tasks, we showed that all of our models are capable of predicting material from emissivity with perfect accuracy, that ResNet18-1D models have the highest (85.9%) top-1 accuracy at shape classification, and random forest models are most effective at size regression, both from an accuracy perspective and given their ability to increase fundamental nanoscience knowledge. Our work shows that automated nanoparticle emissivity spectral analysis with machine learning has the potential to replace more time intensive analytical techniques and can provide more fundamental information about nanoparticle/light interactions.

Note: We open source our code at `https://github.com/chloechsu/nanoparticle`.

References

[1] Ralph A Sperling, Pilar Rivera Gil, Feng Zhang, Marco Zanella, and Wolfgang J Parak. Biological applications of gold nanoparticles. *Chemical Society Reviews*, 37(9):1896–1908, 2008.

[2] Marco Notarianni, Kristy Vernon, Alison Chou, Muhsen Aljada, Jinzhang Liu, and Nunzio Motta. Plasmonic effect of gold nanoparticles in organic solar cells. *Solar Energy*, 106:23–37, 2014.

[3] Emilie Ringe, Mark R Langille, Kwonnam Sohn, Jian Zhang, Jiaxing Huang, Chad A Mirkin, Richard P Van Duyne, and Laurence D Marks. Plasmon length: a universal parameter to describe size effects in gold nanoparticles. *The journal of physical chemistry letters*, 3(11):1479–1483, 2012.

[4] YQ Wang, YG Wang, L Cao, and ZX Cao. High-efficiency visible photoluminescence from amorphous silicon nanoparticles embedded in silicon nitride. *Applied physics letters*, 83(17):3474–3476, 2003.

[5] JA Luna-López, J Carrillo López, I Vivaldo-De la Cruz, G García Salgado, F Flores Gracia, and M Aceves-Mijares. Optical properties of solar cells with sio2 and silicon rich oxide with silicon nanoparticles. *Superficies y vacío*, 23:40–44, 2010.

[6] Mahmoud Elzouka, Charles Yang, Adrian Albert, Sean Lubner, and Ravi S Prasher. Interpretable inverse design of particle spectral emissivity using machine learning. *arXiv preprint arXiv:2002.04223*, 2020.

[7] Vladyslav A Golyk, Matthias Krüger, and Mehran Kardar. Heat radiation from long cylindrical objects. *Physical Review E*, 85(4):046603, 2012.

[8] Jing He, Chang He, Chao Zheng, Qian Wang, and Jian Ye. Plasmonic nanoparticle simulations and inverse design using machine learning. *Nanoscale*, 11(37):17444–17459, 2019.

[9] F. Pedregosa, G. Varoquaux, A. Gramfort, V. Michel, B. Thirion, O. Grisel, M. Blondel, P. Prettenhofer, R. Weiss, V. Dubourg, J. Vanderplas, A. Passos, D. Cournapeau, M. Brucher, M. Perrot, and E. Duchesnay. Scikit-learn: Machine learning in Python. *Journal of Machine Learning Research*, 12:2825–2830, 2011.

[10] Alex Krizhevsky, Ilya Sutskever, and Geoffrey E Hinton. Imagenet classification with deep convolutional neural networks. In *Advances in neural information processing systems*, pages 1097–1105, 2012.

[11] Kaiming He, Xiangyu Zhang, Shaoqing Ren, and Jian Sun. Deep residual learning for image recognition. In *Proceedings of the IEEE conference on computer vision and pattern recognition*, pages 770–778, 2016.

A Supplementary Tables and Figures

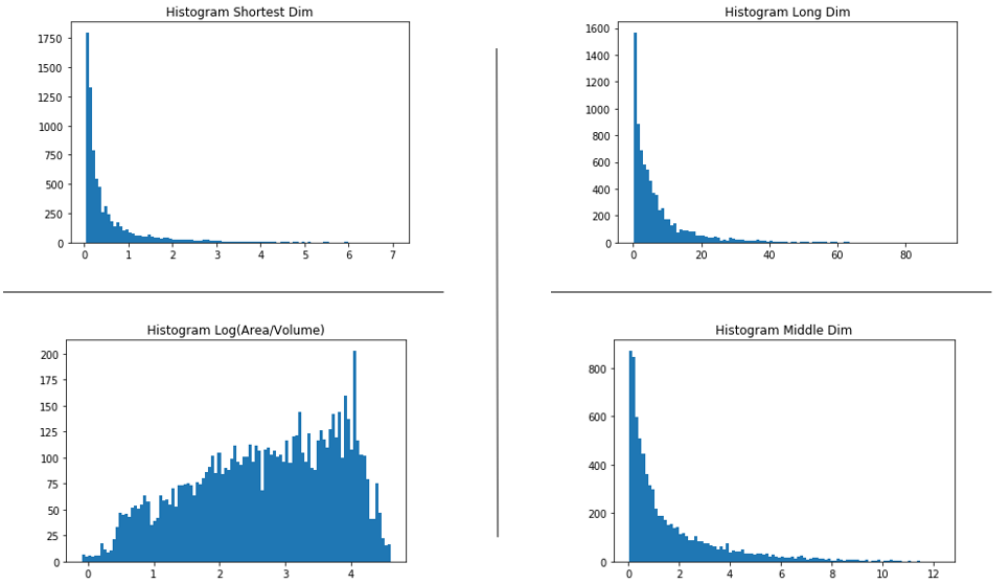

Figure 5: Histogram of size parameters: Log(area/volume), shortest, middle, and longest dimension.

	Classification Top-1 Accuracy				
Model	Triangle Prism	Parallelpiped	Sphere	Wire	Average
Random guess	0.25	0.25	0.25	0.25	0.25
Random forest	0.67	0.54	0.99	0.75	0.74
One-layer neural network	0.412	0.320	0.961	0.525	0.555
Two-layer neural network	0.470	0.286	1.000	0.535	0.573
Three-layer neural network	0.398	0.340	0.961	0.495	0.548
AlexNet-1D	0.486	0.386	1.000	0.780	0.663
ResNet18-1D	0.668	0.590	1.000	0.825	**0.770**
ResNet18-1D (1-channel input)	0.572	0.590	1.000	0.775	0.734

Table 5: Shape classification top-1 accuracies when trained on gold (Au) only.

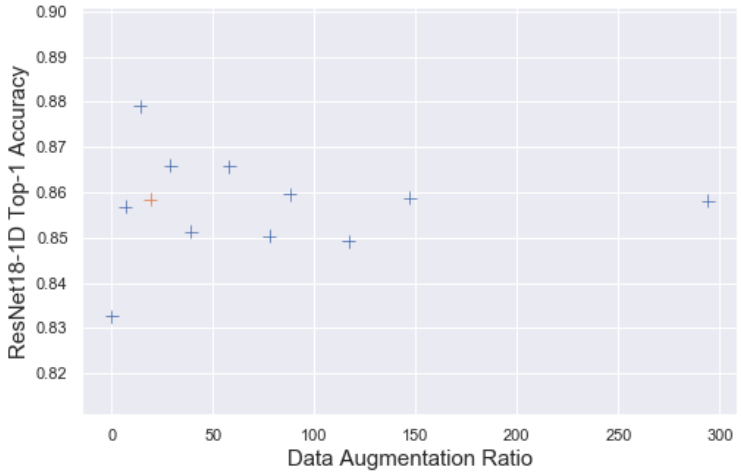

Figure 6: Effects of data augmentation on ResNet18-1D performance. The data augmentation ratio is calculated as (size of augmentation data) / (size of original training data). The red point marks the 20x data augmentation level used in all other experiments.

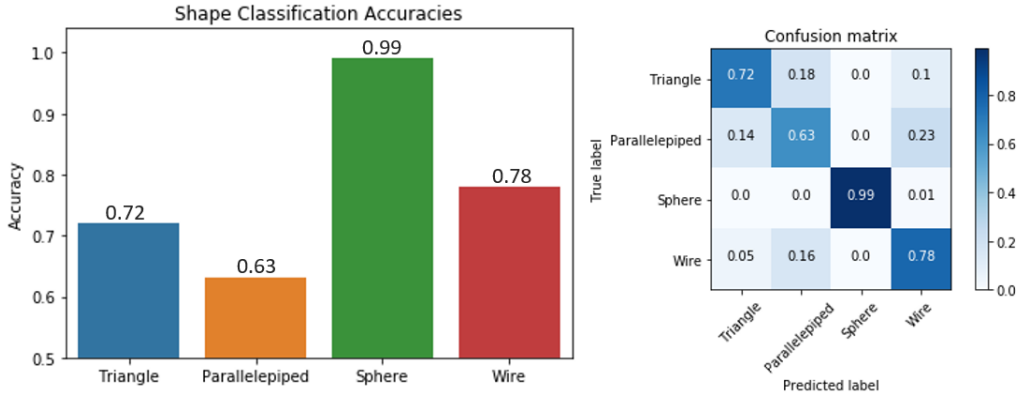

Figure 7: Bar plot showing the accuracy of the random forest multiclass shape classification model at predicting each shape correctly (left) and a confusion matrix for this model (right). Sphere classification was nearly perfect, while there was some confusion between the other three shapes. Wires and Parallelepipeds were particularly likely to be confused as each other.

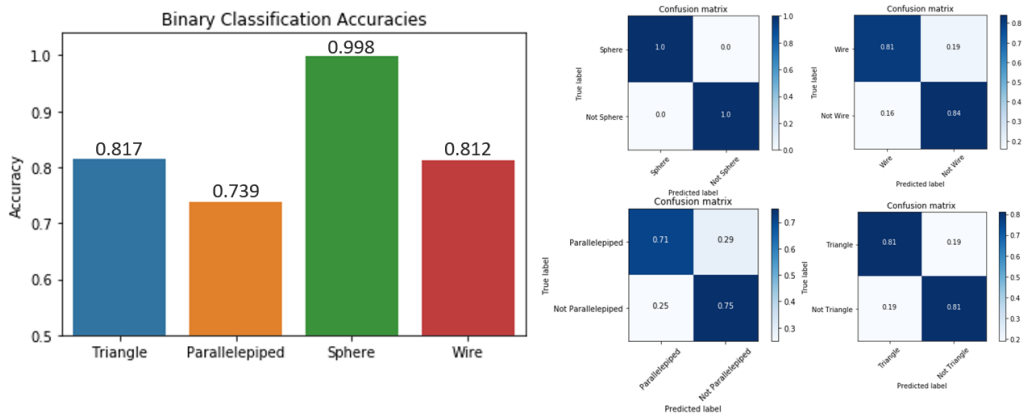

Figure 8: Accuracy and confusion matrices of the four binary classification models. The binary classification models show a high level of accuracy for sphere classification, which approached near perfect accuracy. However, the other shapes were far less accurate. Parallelepiped classification was the worst with an accuracy of 0.739, while the remaining two shapes had accuracies of 0.81. Despite this relatively poorer performance, it should still be noted that all models performed better than a random guess baseline, which would provide an accuracy of 0.5 since our test set contained data where half were of the shape of interest and half were not. The average accuracy across the four models was 0.84.

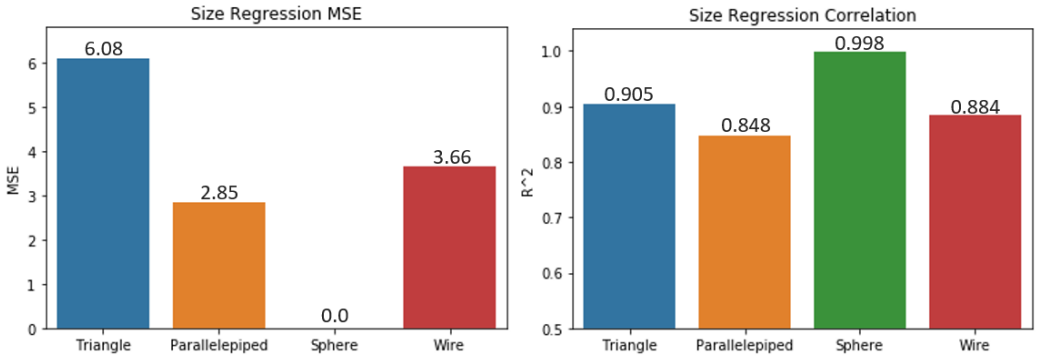

Figure 9: Random forest size regression mean square error (left) and correlation (right) for each shape.

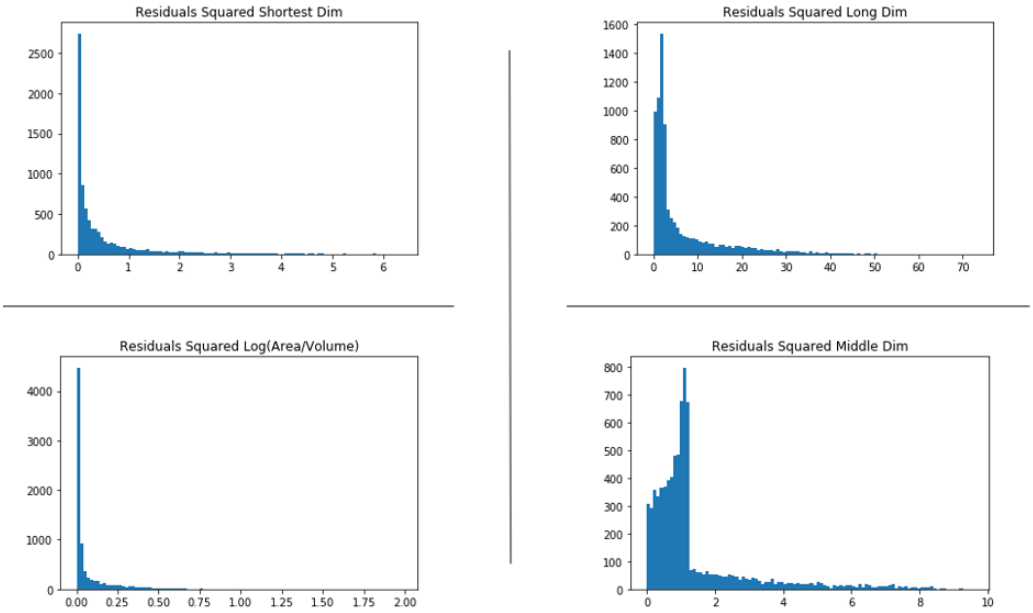

Figure 10: Histogram of the residues in size parameter prediction for the random forest regression model. Log(area/volume) (bottom left), shortest (top left), middle (bottom right), and longest dimension (top right).

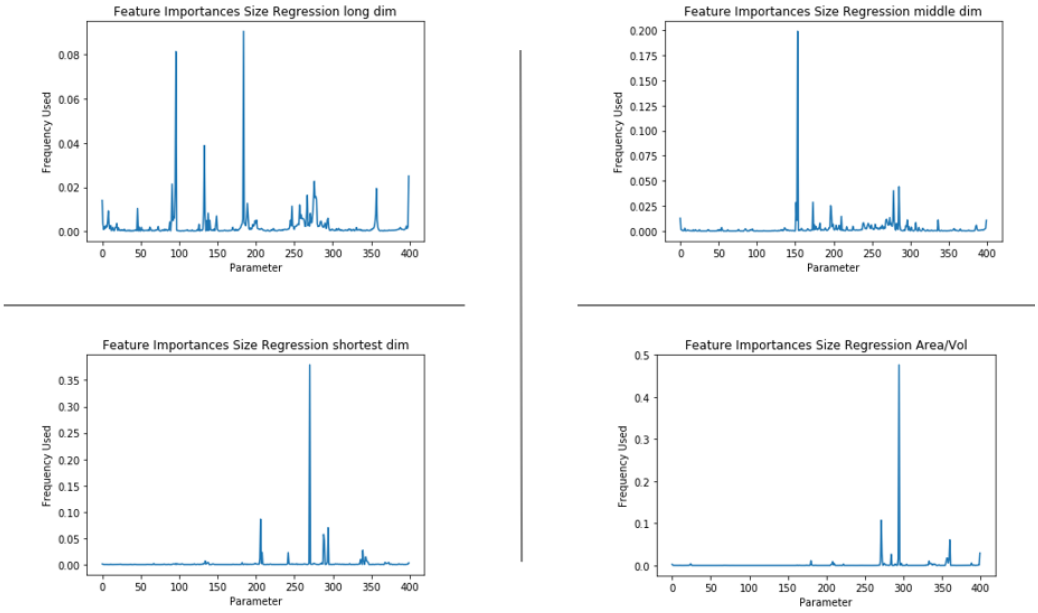

Figure 11: Plot of the feature importances for the random forest size regression models. Each of the parameters represents one of the 400 points that make up a particle's emissivity spectrum and its y axis value shows how important the value at that point is to correctly predicting the size parameter. These four plots show a couple wavelenthgs are very important to determining size, while most of the others are irrelevant. This shows that a couple wavelengths contain most of the information about size prediction, and helps explain random forests success at size prediction. Top left: predict longest dimension. Top right: predict middle dimension. Bottom left: predict shortest dimension. Bottom right: predict log(area/volume)

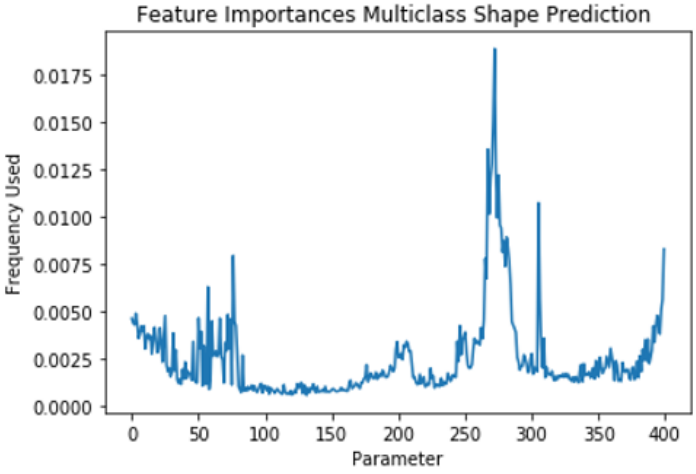

Figure 12: Plot of the feature importances for the shape classification multiclass model. Each of the parameters represents one of the 400 points that make up a particle's emissivity spectrum and its y axis value shows how important the value at that point is to correctly predicting the particle's shape.

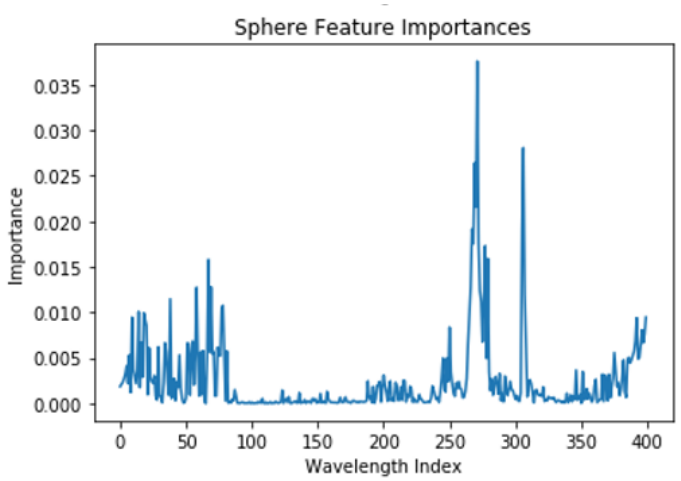

Figure 13: Plot of the feature importances for the random forest sphere binary classification model. Each of the parameters represents one of the 400 points that make up a particle's emissivity spectrum and its y axis value shows how important the value at that point is to correctly predicting the particle's shape.

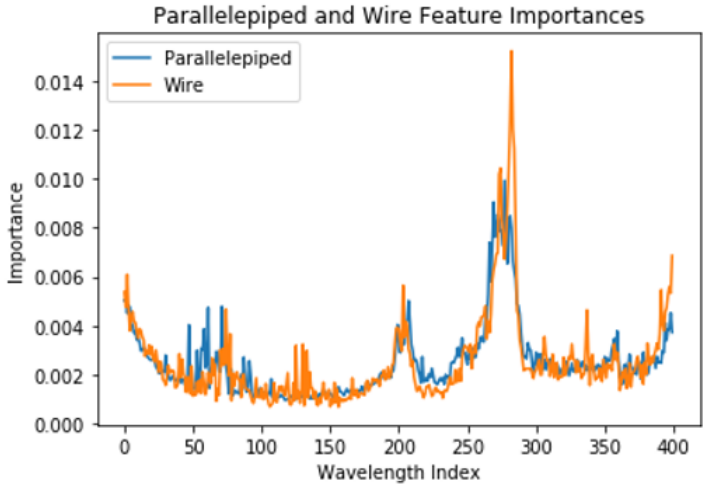

Figure 14: Plot of the feature importances for the random forest wire and parallelepiped binary classification models. Each of the parameters represents one of the 400 points that make up a particle's emissivity spectrum and its y axis value shows how important the value at that point is to correctly predicting the particle's shape. This figure shows how similar the two feature importances are, meaning the models are using many of the same wavelength indices to make predictions.